



Article

Bioassay Directed Isolation, Biological Evaluation and in Silico Studies of New Isolates from *Pteris cretica* L.

Farooq Saleem ^{1,2}, Rashad Mehmood ³, Saima Mehar ⁴, Muhammad Tahir Javed Khan ¹, Zaheer-ud-Din Khan ⁵, Muhammad Ashraf ⁶, Muhammad Sajjad Ali ⁷ , Iskandar Abdullah ⁸ , Matheus Froeyen ⁹, Muhammad Usman Mirza ^{7,9} and Sarfraz Ahmad ^{8,*}

¹ Punjab University College of Pharmacy, University of the Punjab, Lahore 54000, Pakistan

² Faculty of Pharmacy, University of Central Punjab, Lahore 54000, Pakistan

³ Department of Chemistry, University of Education, Vehari Campus, Vehari 61100, Pakistan

⁴ Department of Chemistry, Sardar Bahadur Khan Women University, Quetta 87300, Pakistan

⁵ Botany Department, Government College University, Lahore 54000, Pakistan

⁶ Department of Pharmacy, The Islamia University of Bahawalpur, Bahawalpur 63100, Pakistan

⁷ Institute of Molecular Biology and Biotechnology, University of Lahore, Lahore 54600, Pakistan

⁸ Department of Chemistry, Faculty of Science, University of Malaya, Kuala Lumpur 50603, Malaysia

⁹ Department of Pharmaceutical and Pharmacological Sciences, Rega Institute for Medical Research, Medicinal Chemistry, University of Leuven, B-3000 Leuven, Belgium

* Correspondence: sarfraz.ahmad@um.edu.my; Tel.: +60-111-633-0590

Received: 28 April 2019; Accepted: 24 May 2019; Published: 19 July 2019



Abstract: Members of genus *Pteris* have their established role in the traditional herbal medicine system. In the pursuit to identify its biologically active constituents, the specie *Pteris cretica* L. (*P. cretica*) was selected for the bioassay-guided isolation. Two new maleates (F9 and CB18) were identified from the chloroform extract and the structures of the isolates were elucidated through their spectroscopic data. The putative targets, that potentially interact with both of these isolates, were identified through reverse docking by using in silico tools PharmMapper and ReverseScreen3D. On the basis of reverse docking results, both isolates were screened for their antioxidant, acetylcholinesterase (AChE) inhibition, α -glucosidase (GluE) inhibition and antibacterial activities. Both isolates depicted moderate potential for the selected activities. Furthermore, docking studies of both isolates were also studied to investigate the binding mode with respective targets followed by molecular dynamics simulations and binding free energies. Thereby, the current study embodies the poly-pharmacological potential of *P. cretica*.

Keywords: *Pteris cretica* L.; isolation; molecular docking; neurodegenerative; α -glucosidase; 2,2-diphenyl-1-picrylhydrazyl (DPPH)

1. Introduction

In the history of human civilization, plants have established a role in treating various ailments thereby reducing morbidity and mortality. With the dawn of modern chromatographic and spectroscopic techniques, this rich source of bioactive compounds was and is being extensively studied for the pursuit of high-end medicines. The small-molecule natural products are secondary metabolites of plants biosynthesized mainly as a defense mechanism against pathogenic microorganisms, insects and herbivores [1,2]. From 1981 to 2014, among small-molecule drugs approved by the FDA, 6% were unaltered natural products, 26% natural product derivatives and 27% synthetic drugs which were either a mimic of natural products or have natural product pharmacophores [3].

The genus *Pteris* (*Pteridaceae*) comprises of about 250 species which are widely distributed on all continents excluding Antarctica, with the highest diversity in the tropical and subtropical

area, particularly including New Zealand, Australia, South Africa, Japan, America, China, and Europe [4]. Various species of *Pteris* have long been used for the treatment of different human ailments. *Pteris cretica* L. (*P. cretica*) is among the most commonly used species of *Pteris* in Chinese traditional medicines as an antidote, antipyretic, in burn treatment, antimicrobial and wound healing [5]. Sifting of literature shows that sesquiterpenes, ent-kaurane diterpenes and flavonoids have so far been reported from this plant [6]. We have previously reported the antimicrobial and antioxidant potential of this plant [7]. The current study is an extension of our previously published work. Herein, we report the bioassay-directed isolation and identification of two new isolates (**F9** and **CB18**) from two bioactive subfractions of the chloroform extract of *P. cretica*, along with their structure elucidation, antioxidant, antimicrobial, acetylcholinesterase (AChE) inhibition and α -glucosidase inhibition potentials. The screening of potential molecular targets through reverse in silico studies and the stability and binding free energies are also reported here. The results show that the isolates have moderate potentials for all tested biological activities.

Reactive oxygen species (ROS) produced in our normal metabolic pathway are believed to be responsible for various life-threatening disorders such as cardiovascular disorders, cancer, stress, atherosclerosis, Alzheimer's, Parkinson's, etc. [8,9]. The compounds capable of devouring ROS are termed as antioxidants and could be used as a defense against these life-threatening disorders. Alzheimer's is one of the chronic neurodegenerative diseases characterized by loss of memory, mental abnormality and behavioral instabilities [10,11]. Its prognosis involves the upregulation of acetylcholinesterase (AChE) in the brain cell resulting in diminished amounts of acetylcholine neurotransmitter, which in turn alter smooth brain functions including memory loss. This disorder could possibly be controlled by inhibiting the AChE enzyme, and the candidates capable of this property are called AChE inhibitors. Tacrine, donepezil, rivastigmine and galantamine are commonly used as AChE inhibitors.

The overall scheme for discovering molecular targets of phytochemicals have been uplifted by a variety of in silico tools such as the computer-aided drug discovery [12–16], combinatorial chemistry [17–19] and high throughput screening [20–26]. After identifying lead compounds, directly interacting potential targets are identified using the inverse/reverse docking methodology [27,28] on known crystal structures or using various proteomic tools [29,30]. The target identification approaches involving proteomics profiling and pharmacokinetics studies are laborious and time consuming [31]. Therefore, in silico-based target identification methods are always found as the efficient alternative [32]. Within in silico-based target identification of phytochemicals, various tools are used such as computer-aided drug discovery [13,14], combinatorial chemistry [17,18], high throughput screening [25,26] and large-scale reverse pharmacophore mapping strategy. Among various target prediction tools, the large-scale reverse pharmacophore mapping strategy for potential drug targets identification has appeared to be a potential optional technique [28]. The principle of reverse pharmacophore mapping involves the placement of flexible conformation of every small molecule into every pharmacophore model of proteins in the target list [33]. Presently, various in silico tools have been developed that use different target fishing algorithms to execute reverse docking. Few widely used tools include, PharmMapper [33], ReverseScreen3D [34], INVDOCK [35], Tarfisdock [36], idTarget [37], TargetHunter [38]. By utilizing these in silico tools, various studies have been published, including the identification of molecular targets (i.e., proapoptotic, anti-proliferative, anti-inflammatory, anti-invasive, anti-angiogenic) for tea polyphenols [39], saffron bioactive agents [40], essential oils in cardamom [41] and azadirachtin (the principle bioactive compound of neem seeds) [42].

The present study aimed at the isolation and identification of bioactive constituents from *P. cretica*. The potential molecular targets were screened using the reverse docking procedure. To further investigate the binding pose, the molecular dynamic simulations protocol was employed to analyze the stability and binding free energies of docked complexes. Based on in silico outcomes, selected enzyme inhibition assays were performed along with antibacterial activities. The study revealed the

poly-pharmacological potential of bioactive compounds in *P. cretica*, responsible for its ethnobotanical uses and biological activities.

2. Material and Methods

Column chromatography (CC) was performed on silica gel 60 (70–230 mesh, E. Merck, Darmstadt, Germany). The thin layer chromatography (TLC) was performed on pre-coated silica gel 60 F₂₅₄ plates (E. Merck, Darmstadt, Germany) and the detection was done at 254 and 330 nm or by spraying ceric sulfate in 10% H₂SO₄ (heating). High performance liquid chromatography (HPLC) was performed on the Hitachi Primaide HPLC system (Hitachi, Tokyo, Japan) with C18 columns of Thermo Scientific Hypersil GOLD (5 µm, 175 Å, 4 × 250 mm, Waltham, MA, USA), while the large-scale purification was performed with Thermo Scientific Hypersil GOLD (5 µm, 175 Å, 21.2 × 250 mm). Melting points were measured on a Gallenkamp apparatus (Loughborough, England) and optical rotations were measured on a JASCO DIP-360 polarimeter (Jasco, Tokyo, Japan). UV spectra were recorded on a Hitachi UV-3200 spectrophotometer (Hitachi, Tokyo, Japan) while the FTIR spectra were recorded on a Shimadzu FTIR-8900 spectrometer (Shimadzu, Kyoto, Japan). The ¹H- and ¹³C-NMR spectra were recorded on Bruker AM-400 and AM-500 spectrometers (Bruker BioSpin, Faellanden, Switzerland) in deuterated solvents. The 2D (COSY, HMQC, HMBC) NMR spectra were recorded on the same instruments. The chemical shifts are reported in ppm (δ), relative to the tetramethylsilane (TMS) as an internal standard and the scalar couplings are reported in Hertz (Hz). Mass spectra (MS and HR-MS) in the FAB (fast atom bombardment) mode on Jeol JMS HX 110 spectrometer (Jeol, Tokyo, Japan) were used with glycerol as matrix and ions were given in *m/z* (%). All reagents, solvents and chemicals used were of analytical grade and used without any further purification.

2.1. Plant Collection and Identification

P. cretica whole plant was collected from Azad Kashmir, a state of Pakistan, in April 2013 and identified by Prof. Dr. Zaheer-ud-Din Khan, Department of Botany, Govt. College University, Lahore, Pakistan, where a voucher specimen has been deposited in the herbarium (voucher specimen no. is 2142).

2.2. Extraction and Isolation of Compounds

The whole plants material of *P. cretica* was shade dried (1 kg), ground to powder and extracted with chloroform in a Soxhlet apparatus to dark brown residue (34 g). The residue (34 g) was subjected to column chromatography (CC) over silica gel and eluted with hexane-acetone in order to increase polarity to collect 17 fractions. All the obtained fractions were subjected to measure their antioxidant activity and biological potential against five bacteria. The fractions obtained with 6.5:3.5 and 5.5:4.5 hexane-acetone mixtures were found most active against *S. aureus* and *E. coli* with 37.66%, 17.66% and 38.66%, 16.33% zones of inhibition respectively as compared to the control ampicillin (100% and 94.33%). The fraction obtained with hexane-acetone (1.8:1, 0.5 g) was further purified by CC over silica gel and eluted with dichloromethane (DCM)-methanol mixture in order to increase polarity to collect thirteen subfractions, and all subfractions were subjected to measure their biological activities. The most bioactive subfraction, which was obtained with DCM-methanol (19:1, 135 mg), was rechromatographed over silica gel and eluted with the same solvent system (DCM-methanol) to collect further several subfractions. The most biological active subfraction which was subjected to p-HPLC using water-acetonitrile= 45:55 to 100% acetonitrile to obtain the pure compound (**F9**, 5 mg).

The second bioactive main fraction, which was obtained with hexane-acetone (1.2:1, 1.5 g) was subjected to CC over silica gel and eluted with DCM-methanol in increasing order of polarity to collect 12 subfractions. All the subfractions were subjected to biological activity, the subfraction which was obtained with DCM-methanol (5.7:1, 65 mg) was the most active subfraction, and subsequently this subfraction was subjected to p-HPLC using water-acetonitrile (2:8) to afford the pure compound (**CB18**, 6 mg).

2.2.1. 2-Ethylhexyl Maleate (F9)

Colorless amorphous solid, UV λ_{\max} (MeOH) nm (log ϵ): 285 (2.1). IR ν_{\max} (KBr) cm^{-1} : 3334 (hydroxyl), 2892 br. (carboxylic acid hydroxyl), 1730 (carbonyl), 1653 (conjugated olefin). $^1\text{H-NMR}$ (CDCl_3 , 500 MHz) δ (ppm): 7.68 (1H, d, $J = 9.0$ Hz, H-3), 7.50 (1H, d, $J = 9.0$ Hz, H-2), 4.19 (2H, dd, $J = 14.5, 6.0$ Hz, H-1'), 1.65 (1H, m, H-2'), 1.39 (2H, m, H-1''), 1.32 (2H, m, H-3'), 1.30 (2H, m, H-4'), 1.29 (4H, m, H-5', -6'), 1.26 (2H, m, H-7'), 0.90 (3H, t, $J = 7.5$ Hz, H-2''), 0.86 (3H, t, $J = 7.5$ Hz, H-8'), $^{13}\text{C-NMR}$ (CDCl_3 , 150 MHz) δ (ppm): 167.8 (C-1), 130.9 (C-2), 128.8 (C-3), 167.8 (C-4), 68.1 (C-1'), 38.7 (C-2'), 30.3 (C-3'), 28.9 (C-4'), 29.4 (C-5'), 31.9 (C-6'), 23.0 (C-7'), 14.1 (C-8'), 23.7 (C-1''), 11.0 (C-2''). HR-FAB-MS m/z 257.1747 $[\text{M}+\text{H}]^+$ (calcd. for $\text{C}_{14}\text{H}_{25}\text{O}_4$, 257.1753).

2.2.2. 2-Ethylhexyl Maleate (CB18)

Colorless amorphous solid, UV λ_{\max} (MeOH) nm (log ϵ): 287 (2.2). IR ν_{\max} (KBr) cm^{-1} : 3335 (hydroxyl), 2898 br. (carboxylic acid hydroxyl), 1732 (carbonyl), 1655 (conjugated olefin). $^1\text{H-NMR}$ (CD_3OD , 400 MHz) δ (ppm): 7.72 (1H, d, $J = 8.8$ Hz, H-3), 7.62 (1H, d, $J = 8.8$ Hz, H-2), 4.22 (2H, dd, $J = 5.6, 2.0$ Hz, H-1'), 1.68 (1H, m, H-2'), 1.43 (2H, m, H-1''), 1.36 (2H, m, H-3'), 1.34 (2H, m, H-4'), 1.32 (2H, m, H-5'), 0.94 (3H, t, $J = 7.5$ Hz, H-6'), 0.91 (3H, t, $J = 7.2$ Hz, H-2''). $^{13}\text{C-NMR}$ (CD_3OD , 150 MHz) δ (ppm): 169.4 (C-1), 132.4 (C-2), 129.9 (C-3), 169.4 (C-4), 69.1 (C-1'), 40.2 (C-2'), 31.6 (C-3'), 30.1 (C-4'), 24.0 (C-5'), 14.4 (C-6'), 24.9 (C-1''), 11.4 (C-2''). HR-FAB-MS m/z 229.1430 $[\text{M}+\text{H}]^+$ (calcd. for $\text{C}_{12}\text{H}_{21}\text{O}_4$, 229.1440).

2.2.3. In Silico Drug Likeness and ADMET Properties of Active Compounds in *P. cretica*

In order to check the drug-like potential of active compounds in *P. cretica*, physicochemical properties were determined from Mcule (<https://mcule.com/>) [43]. Drug-likeness and the drug score of the compounds, which is based on topological descriptors, fingerprints of molecular drug likeness, structural keys or other properties as $\log P$ and molecular weights were determined from the Molinspiration program (<http://www.molinspiration.com/cgi-bin/properties>) and Osiris Property Explorer (<http://www.organic-chemistry.org/>). Detailed ADMET (Absorption, Distribution, Metabolism, Excretion and Toxicity) were predicted from the admetSAR webserver (<http://lmmd.ecust.edu.cn:8000/predict/>) [44].

2.3. Identification of Putative Therapeutic Target

To find the potential therapeutic targets for active compounds of *P. cretica*, dual reverse screening approaches were employed by using the ReverseScreen 3D [34] and PharmMapper webserver [33]. ReverseScreen 3D screens the potential targets against biological active small compounds from the updated subsets of co-crystallized ligands present in the Protein Data Bank (PDB). PharmMapper is another reverse screening webserver, which employs pharmacophore-mapping strategy for the identification of potential targets for given small compounds. PharmMapper carries a large, internal database namely PharmTargetDB annotated from all the target information in BindingDB [45], DrugBank [46] and the potential drug target database (PDTD) [47]. Active compounds from *P. cretica* were submitted to the ReverseScreen 3D and PharmMapper in the default format. The list of potential targets was further investigated to filter out the targets associated to anticancer, antioxidant, anti-inflammatory, and neurodegenerative mechanisms. The high throughput experimental findings of potential targets were manually curated from three different bioassay databases: PubChem Bioassay [48], NPACT [49] and Herbal Ingredients' Targets Database [50]. The list of potential targets identified by the in silico reverse screening method was compared with the target information acquired from three bioassay databases as an experimental evidence. Based on the results, various identified targets such as anti-proliferative, antioxidant and anti-inflammatory targets were sorted out. Alongside the reverse docking, the antibacterial efficacy of the identified compounds was also evaluated by carefully taking into account the potential antibacterial targets after literature review.

2.4. Experimental Protocols for Biological Assays

To validate the therapeutic targets identified by the in silico reverse docking procedure, various biochemical assays were performed.

2.5. Antibacterial Assay

The antibacterial potential of isolated compounds **F9** and **CB18** was measured against Gram-negative *Escherichia coli* (*E. coli*), *Shigella flexneri* (*S. flexneri*), *Pseudomonas aeruginosa* (*P. aeruginosa*) and *Klebsiella pneumoniae* (*K. pneumoniae*), and Gram-positive *Staphylococcus aureus* (*S. aureus*) bacteria by using a Microplate Alamar Blue Assay (MABA) [51]. The selected bacteria were taken from the Pakistan Council of Scientific and Industrial Research (PCSIR) laboratory, Lahore, Pakistan. Muller Hinton media (MHM) was used for bacterial culturing and 0.5 McFarland turbidity index was maintained for inoculums. MHM (50 μ L) was inoculated to each well of 96-well microtiter plate under sterile conditions. A volume of 10 μ L from each test sample was pipetted into all labelled wells excluding control wells. Each well was added with MHM to make a final volume of 200 μ L. A specific bacterial suspension with a volume of 7 μ L (5×10^6 cfu/mL) was added to all wells in the plate. To avoid a dehydration issue in bacteria, parafilm was used to cover the microplate and then placed for incubation at 35 °C for 18 to 20 h. At this phase, the microplate contained a set of samples, standard and a negative control. Next to the incubation period, a multichannel pipette was used to pipette 10% resazurin (dye) to total culture volume into each well. Now the microplate was mixed with a speed of 80 rpm in a shaking incubator for 2 to 3 h. During the blending process, it was ensured that the parafilm remained attached with the plates. The change in color from blue to pink was the assessment of bacterial growth (viability).

The diminution in blue color concentration was measured with the ELISA reader at 570 nm and 600 nm wavelengths. The percentage inhibition was calculated with the following formula and repeated thrice to find the mean inhibition and standard deviation.

$$\% \text{ Difference} = \frac{(\epsilon_{\text{ox}}) \lambda_2 A \lambda_1 - (\epsilon_{\text{ox}}) \lambda_1 A \lambda_2 \text{ of test agent dilution}}{(\epsilon_{\text{ox}}) \lambda_1 \text{Å} \lambda_2 - (\epsilon_{\text{ox}}) \lambda_2 \text{Å} \lambda_1 \text{ of untreated positive growth control}} \times 100$$

where, ϵ_{ox} is the molar extinction coefficient of Alamar blue oxidized form (blue), A is the absorbance of the test well, Å is the absorbance of the positive growth control well, λ_1 is the wavelength at 570 nm and λ_2 is the wavelength at 600 nm.

2.6. Antioxidant Activity

Stock solutions of test compounds **F9** and **CB18** and standard vitamin C were prepared in ethanol at a concentration of (1 mg/mL). Each well of 96-well microtiter plate was loaded with 50 μ L of ethanol. The serial dilutions (128, 64, 32, 16, 8, 4, 2, 1, 0.5, 0.25, 0.125 μ g/mL) were prepared by using 50 μ L of stock solution. The ethanolic solution of DPPH (150 μ L, 0.05 mM) was added to each well. Control wells contained 50 μ L ethanol and 150 μ L DPPH solution. The plate was incubated for 30 min in the dark and the absorbance was read at 517 nm. The antioxidant activity was expressed as the percentage radical scavenging activity (%RSA) and calculated by using the following expression.

$$\% \text{RSA} = (\text{Ac} - \text{As}) / \text{Ac} \times 100$$

where, Ac and As are the absorbance of control and sample, respectively. The experiment was repeated thrice to find the mean %RSA \pm standard deviation and IC_{50} was calculated by plotting the log of concentration against the mean %RSA.

2.7. Acetylcholinesterase (AChE) Inhibition Activity

The AChE inhibition potential of isolates was investigated according to the reported procedure with slight modifications [52]. The methanolic solution of the test compound or standard (Eserine) (10 μ L, 0.5 mM) was added to 96-well plates containing 60 μ L phosphate buffer (pH = 7.7, 50 mM). Control wells contained 60 μ L phosphate buffer and 10 μ L methanol. This was followed by loading 10 μ L enzyme (0.005 units for AChE) to each well. The wells contents were shaken and the absorbance at 405 nm was measured. The plate was incubated at 37 °C for 10 min and the substrate (acetylthiocholine iodide) (10 μ L, 0.5 mM) and 5, 5-Dithio-bis-(2-Nitrobenzoic Acid) (10 μ L, 0.5 mM) were added to each well. The plate was incubated for 15 min at 37 °C and the absorbance was measured at 405 nm using a 96-well plate reader. The test was repeated in triplicate and the percentage inhibition was calculated by following the formula.

$$\% \text{ Inhibition} = (Ac - As)/Ac \times 100$$

2.8. α -Glucosidase (GluE) Inhibition Assay

α -Glucosidase (GluE) inhibition assay was carried out with slight modifications in the method performed by Chapdelaine [53]. The wells of the 96-well microtiter plate were loaded with 70 μ L phosphate buffer saline (50 mM, pH = 6.8) and the test samples or Acarbose as standard (10 μ L, 0.5 mM). The control wells contained 70 μ L phosphate buffer and 10 μ L methanol. A volume of 10 μ L GluE enzyme (0.057 units) was pipetted into each well followed by proper mixing. After 15 min of pre-incubation period (at 37 °C), the absorbance was recorded at 400 nm. For the initiation of reaction, 10 μ L of p-nitrophenyl glucopyranoside (0.5 mM) was added as the substrate. The plate was incubated for 30 min at 37 °C before measuring the absorbance at 400 nm. The percentage inhibition was calculated by the same following formula and the experiment was repeated in triplicate to find the mean and standard deviation.

$$\% \text{ Inhibition} = (Ac - As)/Ac \times 100$$

2.9. Molecular Docking of Potential Targets with Bioactive Compounds

To investigate the binding mode and molecular interactions of investigated compounds with therapeutic targets as identified with the experimental procedure, molecular docking studies was employed using Autodock Vina with default setting and parameters [54]. The X-ray determined crystallographic 3D structures of identified potential targets including AChE (PDB ID: 4BDT), based on the mechanism involved in neurodegeneration were retrieved from PDB with a good resolution and R-free factor [55] while *Saccharomyces cerevisiae* α -glucosidase enzyme was modeled using *Saccharomyces cerevisiae* isomaltase (PDB ID: 3AJ7, Identity: 72.4%) as a template due to the unavailability of crystal structure. SWISS-MODEL [56] was utilized for homology modeling and the model was refined through 20 ns MD simulations. For antimicrobial targets, an extensive literature review was performed and the dihydropteroate synthase (DHPS) from *Escherichia coli*, and dihydrofolate reductase (DHFR) from *Staphylococcus aureus* were selected for docking studies and there the corresponding PDB IDs were 5U10 (*E. coli* DHPS complex with pteronic acid) [57] and 4LAE (*S. aureus* DHFR complex with 7-(Benzimidazol-1-yl)-2,4-diaminoquinazolines) (PDB ID: 4LAE) [58].

For the structure preparation, co-crystallized ligands were separated from the corresponding proteins and re-docked again to calculate the RMSD of docked and co-crystallized ligand for reliability of the AutoDock Vina protocol [54]. The overall protocol of the protein preparation, minimization and optimization has been distinctively described elsewhere [59–61]. The molecular structures of potent bioactive compounds **F9** and **CB18** were generated from the ACD/ChemSketch Freeware, the software was employed to design the 2D structure and OpenBabel was used to convert 2D to 3D structure. AutoDock Tools were used to merge non-polar hydrogens, add Gasteiger charges and rotatable bonds adjustments. The docked complexes were investigated for molecular interactions utilizing UCSF Chimera v10 [62].

2.10. Molecular Dynamics Simulations and Binding Free Energy Calculations

To understand the dynamic behavior with respect to time (nanoseconds, ns), the best-docked complexes from molecular docking studies were executed through 20 ns MD simulations. All MD simulations were executed using the AMBER 16 package [63]. We implemented the same MD simulation protocol as described in our previous study [64]. The CPPTRAJ module of AMBER 16 [65] was used for the trajectory analysis.

To further explore the binding free energy calculations between selected proteins with bioactive compounds separately. A total of 500 snapshots were extracted from the whole trajectory for binding free energy calculations using the molecular mechanics-generalized Born surface area (MMGBSA) method. MMGBSA calculations were performed using the mmpbsa module of AMBER 16 package. The details of the MMGBSA method have been explained elsewhere [66,67]. The MMGBSA total energy (ΔG_{tot}) was divided into molecular mechanics (ΔE_{MM}) and solvation energy (ΔG_{sol}) contributions. ΔE_{MM} is further divided into electrostatic energy contributions (ΔE_{ele}) and van der Waals (ΔE_{vdw}) while the solvation energy is divided into polar (ΔG_{p}) and nonpolar (ΔG_{np}) contributions.

$$\begin{aligned}\Delta E_{\text{MM}} &= \Delta E_{\text{int}} + \Delta E_{\text{ele}} + \Delta E_{\text{vdw}} \\ \Delta G_{\text{sol}} &= \Delta G_{\text{p}} + \Delta G_{\text{np}} \\ \Delta G_{\text{tot}} &= \Delta E_{\text{MM}} + \Delta G_{\text{sol}}\end{aligned}$$

3. Results and Discussion

In our previous study on *P. cretica*, n-hexane, chloroform and ethanol extracts of the whole plant were screened for antimicrobial and antioxidant activities. The chloroform extract was found the most active among all studied extracts [7]. The current study was commenced to isolate the active ingredients from the chloroform extract. The shade dried whole plant was ground and extracted with chloroform using the Soxhlet extractor. The crude extract was subjected to repeated column chromatography steps, each followed by biological activates of fractions in a bioassay-guided manner to identify the most active fractions. After column chromatography steps, most active fractions were subjected to the reverse phase HPLC to isolate the pure ingredients.

Compound **F9** was obtained as a white amorphous powder. The UV spectrum showed the absorption bands at 285 nm, while the IR spectrum exhibited absorptions for the presence of hydroxyl (3334 cm^{-1}), carboxylic acid hydroxyl (2892 br. cm^{-1}), carbonyl (1732 cm^{-1}), and olefinic (1655 cm^{-1}) moieties. The molecular formula was deduced as $\text{C}_{14}\text{H}_{25}\text{O}_4$ by high resolution FAB-MS (fast atom bombardment-mass spectrum), which showed the pseudo molecular ion $[\text{M}+\text{H}]^+$ peak at m/z 257.1747. Two downfield doublets of $^1\text{H-NMR}$ spectrum of **F9** (Table 1) of olefinic protons at δ 7.68 and 7.50 with coupling constant 9.0 Hz revealed the presence of olefinic bond having *cis* geometry. A methylene proton signal at δ 4.19 (dd, $J = 14.5, 6.0$ Hz) showed its connectivity with oxygen and methine multiplet at δ 1.65 (1H, m) in COSY. The high frequency region was a characteristic of hydrocarbon chain methylenes within the range of δ 1.29–1.39 (12H) and the presence of two terminal methyl groups was revealed by two triplets at δ 0.90 (t, $J = 7.5$ Hz) and 0.86 (t, $J = 7.5$ Hz), which indicated the presence of a branch in the hydrocarbon chain. $^{13}\text{C-NMR}$ (BB and DEPT) spectra showed the carbonyl carbons signal at δ 167.8 while the olefinic carbons showed signals at δ 130.9 and 128.9. The oxygenated methylene carbon was observed at δ 68.1 whereas a methine carbon showed the signal at δ 38.1. The methylene carbons of the hydrocarbon chain were resonated in the range of δ 23.0–31.9 with the two terminal methyl signals at δ 14.1 and 11.0.

Table 1. Potential therapeutic targets of isolates **F9** and **CB18** identified by PharmMapper and ReverseScreen3D.

Drug Target Proteins	F9		CB18		Experimental Evidence
	Target Hit	Fit Score	Target Hit	Fit Score	
EGFR	✓	3.48	✓	4.96	PubChem Bioassay
Estrogen receptor beta	n.a	n.a	✓	3.996	NPACT
Cytochrome P450 2C9	✓	4.22	n.a	n.a	NPACT
Acetylcholinesterase (AChE)	✓	4.52	✓	4.3	PubChem Bioassay
TGF-beta receptor type-1	✓	3.75	n.a	n.a	Drug Bank
phosphodiesterase-5 (PD-5)	✓	4.72	n.a	n.a	Drug Bank
Cell dependent kinase 2	n.a	n.a	✓	2.65	PubChem Bioassay
Caspase 3	✓	4.67	✓	5.02	NPACT
Deoxycytidine kinase	✓	2.66	n.a	n.a	Drug Bank
human carboxylesterase (hCE-1)	✓	3.87	n.a	n.a	PubChem Bioassay
Fibroblast growth factor receptor 1, FGFR1	✓	3.41	✓	4.96	PubChem Bioassay
Caspase 7	✓	2.41	n.a	n.a	PubChem Bioassay
STAT-3	✓	4.93	✓	5.39	PubChem Bioassay
Cyclin dependent kinase 6	✓	3.81	✓	4.34	Drug Bank
Cyclin A2	n.a	n.a	✓	3.95	NPACT
p53	✓	4.19	n.a	n.a	Drug Bank
glycogen synthase kinase-3 β (GSK-3 β)	✓	4.17	✓	3.5	Drug Bank
Apoptosis regulator Bcl-X	✓	4.88	n.a	n.a	PubChem Bioassay
nitric oxide synthase (NOS)	✓	3.39	✓	3.1	PubChem Bioassay
vascular endothelial growth factor, VEGF	✓	3.44	✓	4.18	PubChem Bioassay
MAP kinase 14	✓	3.63	n.a	n.a	NPACT
Histone deacetylase 8	✓	4.26	✓	4.21	PubChem Bioassay
Tumor necrosis factor-alpha	✓	5.34	✓	4.97	PubChem Bioassay
NF- κ B	n.a	n.a	✓	2.94	PubChem Bioassay
Prothrombin	n.a	n.a	✓	4.09	Drug Bank
Ornithine aminotransferase, mitochondrial	✓	3.78	✓	2.97	PubChem Bioassay
Sepiapterin reductase	✓	4.81	n.a	n.a	NPACT
VEGFR2	✓	5.11	✓	4.62	PubChem Bioassay
Cyclin dependent kinase 4	n.a	n.a	✓	2.54	Drug Bank
cyclooxygenase-2, COX2	✓	4.14	✓	5.39	Drug Bank
3-phosphoinositide-dependent protein kinase 1	n.a	n.a	✓	4.41	PubChem Bioassay
Beta-secretase 1	✓	3.18	✓	4.39	Drug Bank
JNK1	✓	2.86	✓	3.47	PubChem Bioassay
RAC-alpha	✓	4.55	n.a	n.a	PubChem Bioassay
serine/threonine-protein kinase	✓	3.97	✓	4.58	PubChem Bioassay
Estradio 17-beta dehydrogenase-1	✓	2.67	n.a	n.a	PubChem Bioassay
Interleukin- 4	✓	2.67	n.a	n.a	PubChem Bioassay

In COSY correlations of F9 (Figure 1), the proton at δ 4.19 (H-1') showed the COSY correlation with the proton at δ 1.65 (H-2'), which subsequently showed a correlation with the proton at δ 1.39 (H-1'') and δ 1.32 (H-3'), revealing the presence of the branch at C-2'. In the HMBC experiment (Figure 1), olefinic protons at δ 7.68 and 7.50 showed 2J and 3J correlations with the carbonyl at δ 167.8, confirming the presence of olefinic bond adjacent and in conjugation with the carbonyls. The proton at δ 4.19 (H-1') showed the 3J correlations with carbonyl carbon at δ 167.8 (C-4), which confirms the presence of ester moiety and connectivity of C-1' with ester oxygen. The proton at δ 4.19 (H-1') also showed 3J with δ 30.3 (C-3') and 23.7 (C-1''), and 2J correlation at δ 38.1 (C-2'), and subsequently H-2' (δ 1.65) showed key 2J correlations at δ 30.3 (C-3') and 23.7 (C-1'') and 3J correlation at δ and 11.0 (C-2''), confirming the branch is ethyl group and its connectivity at C-2'. The remaining HMBC correlations illustrated in Figure 1 along with COSY correlations were in complete agreement with the assigned structure of compound **F9** as 2-ethyloctyl maleate (Figure 1).

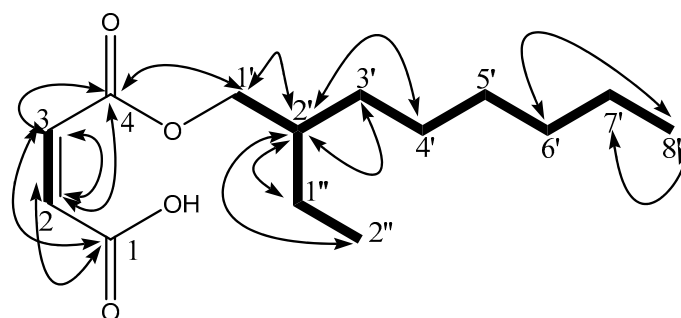


Figure 1. Structure of compound **F9** (2-ethyloctyl fumarate) with important ¹H-¹H COSY (—) and ¹H-¹³C HMBC (→) correlations.

Compound **CB18** was also obtained as a white amorphous powder. The UV and IR spectra were similar to those of compound **F9**. HR-FAB-MS showed the pseudo molecular ion $[M+H]^+$ peak at m/z 229.1433 consistent to the molecular formula $C_{12}H_{21}O_4$. Compound **CB18**, therefore, differed from compound **F9** in having two methylene groups less in the hydrocarbon chain, as $[M+H]^+$ peak of compound **CB18** was m/z 28 less to that of compound **F9**. The ¹H and ¹³C NMR spectra showed common features resemblance to those of compound **F9**, allowing to assign the structure of compound **CB18** as 2-ethylhexyl maleate (Figure 2).

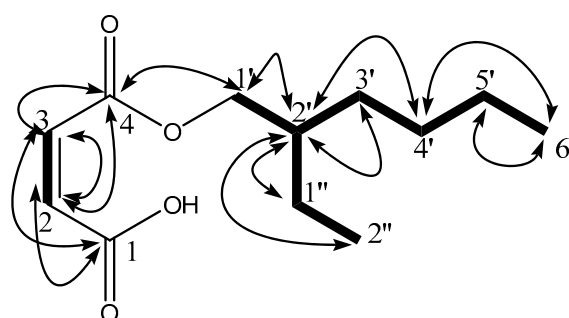


Figure 2. Structure of compound **CB18** (2-ethylhexyl fumarate) with important ¹H-¹H COSY (—) and ¹H-¹³C HMBC (→) correlations.

3.1. Putative Therapeutic Target for Isolates

The list of potential top-ranked targets predicted from PharmMapper and ReverseScreen3D were tabulated in Table 1. Most of these targets are associated to anticancer, anti-inflammatory and neurodegenerative mechanisms as demonstrated in proceeding sections. The pharmacokinetics/ADMET estimations of both bioactive compounds are tabulated in Supplementary Table S1.

3.2. Antiproliferative Targets

The process of growth and differentiation is under tight regulation, controlled by growth factors and their receptors. Abnormal growth and development may result as a consequence of slight variations in the regulation of expression of the molecules associated, causing malignant transformation. An increase in the expression level of growth factors for instance, transforming growth factor- α (TGF- α), can lead to non-cancerous disease, one such example is psoriasis. Anticancer studies have demonstrated a significant role of growth factors regarding anticancer activity [68]. Proliferation of a cancerous cell has portrayed an over-expression of the epidermal growth factor receptor (EGFR) as a prominent factor [68–70]. Two distinct signaling pathways regulate the apoptotic process which forms a loop-structure after their merger as a result of the effector molecule, Caspase 3 activation [71]. Reverse Screening has helped us to figure out various growth factors that can act as potential targets for bioactive compounds identified in *P. cretica*. The basic fibroblast growth factor receptor 1 and placental

growth, epidermal growth factor receptor and VEGFR2 were estimated to bind with both compounds. The anti-angiogenesis potential of *P. cretica* might be central to the binding to these growth factors. The proapoptotic activity has been linked with these bioactive compounds, which bind to BCL-XL, Caspase 3 and Caspase 7 for further activation. Cyclins play a key role in different phases of a cell cycle. Three types of cyclins (cyclin D1, cyclin D2, cyclin D3) bind to CDK4 and to CDK6 and CDK-cyclin D complexes to regulate the entry in the G1 phase [72,73]. This study identified that the proliferation inhibition can be brought about by targeting Cyclin-A2 and cyclin dependent kinases 2 causing G1 cell cycle arrest through **CB18** and **F9**. This process promotes apoptotic cell death and hence, estimated the onco-protective potential of *P. cretica*. As tabulated in Table 1, a set of other targets including MAP kinase 14, Estrogen receptor Beta, p53, revealed **CB18** and **F9** of significant importance with respect to cancer-preventive potential of *P. cretica*.

3.3. Antioxidant and Antiinflammatory Targets

Studies centered upon carcinogenesis have indicated inflammation to be of prime importance in the process, involving tumor initiation, promotion and its progression. Acute inflammation though observed to play a significant role in defense response, cancer has been found to be caused by chronic inflammation [74]. For their role in the inhibition of proliferation, angiogenesis, invasion and metastasis, pro-inflammatory gene products have been in the spotlight over the last two decades [75]. Studies have demonstrated that the progression of various forms of cancer involves key components of inflammatory pathways such as cytokines, signal transducer and activator of transcription-3 (STAT-3), prostaglandins, free radicals, vascular endothelial growth factor (VEGF), NF- κ B, cyclooxygenase-2 (COX-2) and inducible nitric oxide synthase (iNOS) [76,77]. In the progression of inflammation, in controlling the factors that deal with the immune cells, the tumor necrosis factor (TNF) has a significant contribution, which was estimated as a potential target identified for both bioactive compounds of *P. cretica*. The current reverse screening protocol, has revealed many anti-inflammatory targets including Tumor necrosis factor, Estradio 17-beta dehydrogenase-1, cyclooxygenase-2, Interleukin- 4 and VEGFR that have the potential to bind with **CB18** and **F9**, key bioactive compounds of *P. cretica*.

3.4. Neurodegenerative Mechanism

Neurodegeneration being multi-factorial represents a complex pathogenesis. One of the neurodegenerative disorders, Alzheimer's disease (AD), is characterized by the development of plaques formed by the aggregation of beta-amyloid ($A\beta$) peptide, responsible for causing neuronal death [78]. Amyloid precursor protein (APP) that undergoes a cleavage by β -secretase, is an attractive target for developing potent inhibitors. Furthermore, secretases that cleave amyloid precursor protein are thought to be potential targets for inhibiting APP cleavage [79]. It has been hypothesized that $A\beta$ protein accumulates inside the brain causing neurons to die. Hence, the inhibition of $A\beta$ aggregation and deposition by inhibiting COX 1 and 2 is considered to play a significant role in treating neuronal damage [80,81]. Neurofibrillary tangles formed as result of Tau protein phosphorylation have been found to contribute towards progression of neurodegeneration through paired helical filament-tau (PHF-tau) production. It has been observed that dephosphorylation caused by kinases: Glycogen synthase kinase-3 β (GSK-3 β), cyclin-dependent protein kinase 5 (cdk5) and c-Jun N-terminal kinases (JNKs), alleviates cognitive decline [82,83]. Cholinesterases, specifically, acetylcholinesterase (AChE) and butyrylcholinesterase (BuChE) are responsible for the catalytic hydrolysis of important neurotransmitter acetylcholine and butyrylcholine, respectively [84]. Moreover, the inhibition of human carboxylesterase (hCE-1) being similar in structure to cholinesterases (ChE) is also considered as an effective strategy [85]. Oxidative stress has been linked to the neuronal cell death since long. The induction of nitric oxide (NO) produced by nitric oxide synthase (NOS) has been found to play a role in oxidative damage linked to neurodegeneration [86]. Pro-inflammatory cytokines have been found responsible for neuroinflammation leading to neurodegeneration of which TNF- α tops the list [87]. To enhance neuroprotection and cognitive function, the inhibition of phosphodiesterase-5 (PD-5) has

been found useful [88]. All above-mentioned targets are perfectly identified by bioactive compounds (CB18 and F9) which estimated the neuroprotective potential of *P. cretica* (Table 1).

3.5. Biological Activities of Isolates

Due to experimental and financial constraints, some of the identified targets were selected to evaluate the potential of bioactive compounds from *P. cretica* against antibacterial and enzymatic inhibition activities. To further estimate the therapeutic potential, other identified targets were taken into account and investigated through molecular modeling studies.

3.6. Antibacterial Activities

The antibacterial activities of two isolated compounds were performed against selected bacteria by applying MABA and results have been reported in Table 2.

Table 2. Antibacterial activities (% inhibition) of isolates from *P. cretica* and standard ampicillin at 1 mg/mL. Each value is average of three repeated experiments \pm standard error (S.E.).

Compounds	<i>E. coli</i>	<i>S. aureus</i>	<i>K. pneumoniae</i>	<i>S. flexneri</i>	<i>P. aeruginosa</i>
F9	11.33 \pm 0.66	14.00 \pm 0.57	-	-	-
CB18	14.33 \pm 0.33	10.00 \pm 0.00	-	-	-
Ampicillin	90.67 \pm 0.66	95.00 \pm 0.00	80.00 \pm 0.00	90.66 \pm 0.66	91.33 \pm 0.88

For testing of antibacterial activity of isolated compounds, MABA was employed and results have been tabulated in Table 1. The compounds F9 and CB18 did not demonstrate any activity against *K. pneumoniae*, *S. flexneri* and *P. aeruginosa* whilst showed less significant antibacterial activity against *E. coli* (i.e., 11.33% and 14.33%) and *S. aureus* (i.e., 14% and 10%) as compared to ampicillin at 1 mg/mL.

3.7. Antioxidant Activities

Purified compounds were subjected to test their antioxidant potential by the DPPH assay and the results have been tabulated in Table 3.

Table 3. Antioxidant activity of isolated compounds. Each value represents IC_{50} of average of three repeated experiments \pm standard error (S.E.).

Ser. No.	Compounds	DPPH (IC_{50}) mM
1	F9	02.17 \pm 0.49
2	CB18	02.93 \pm 0.51
3	Vitamin C	0.029 \pm 0.47

All isolates exhibited IC_{50} in millimolar (mM) range. Their results were not promising as compared to vitamin C. This effect could stem from the absence of any functional groups capable of reduction.

3.8. Enzyme Inhibition Activities

The isolated compounds were also studied for their enzyme inhibition potential against AChE and GluE. The results in terms of percentage inhibition have been mentioned in Tables 4 and 5.

Table 4. AChE inhibition activities of isolates (F9 & CB18) at 0.5 mM with Eserine as standard. The values represent average percentage inhibition \pm standard error (S.E.) of three repeated experiments.

Ser. No.	Compounds	Inhibition (%) at 0.5 mM AChE
1	F9	N.D.
2	CB18	13.25 \pm 0.14
3	Eserine	91.27 \pm 1.17

N.D. = not detected.

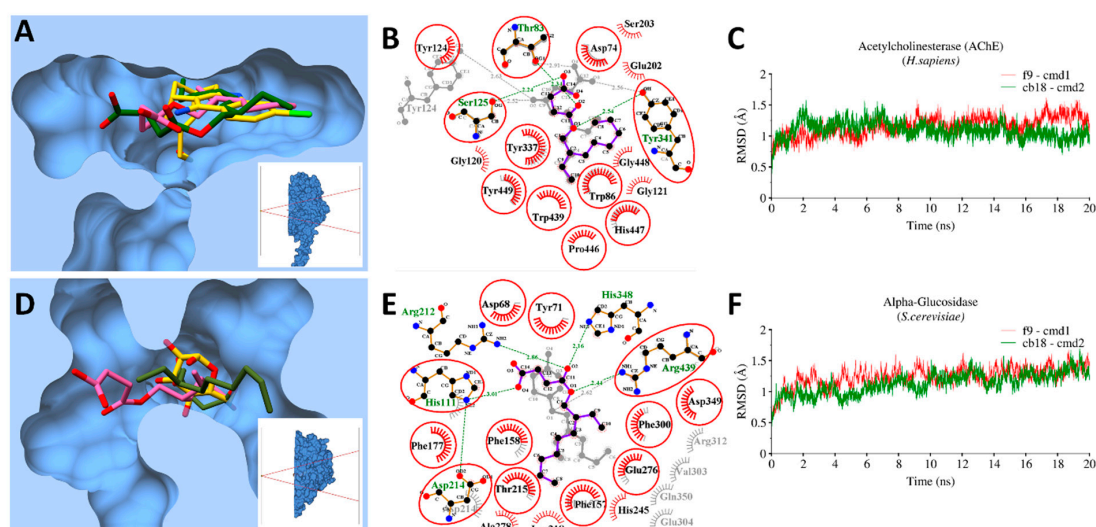


Figure 4. Molecular interactions and MD simulations of **CB18** and **F9** against AChE and *S. cerevisiae*- α -glucosidase. (A) The molecular surface representation of acetylcholinesterase (AChE) with bound co-crystallized ligand (gold), **CB18** (green) and **F9** (pink) superimposed together; (B) 2D-interaction plots with AChE after MD-simulations, hydrophobic interacting residues are labeled black with spiked red arc, while those interacting through H-bonds are labelled green with distance in angstrom. Conserved residues are marked with red circles; (C) RMSD trajectory plots of AChE with bound **CB18** (green) and **F9** (red) over a period of 20 ns. The same representation of corresponding *S. cerevisiae*- α -glucosidase with bound **CB18** and **F9** are displayed in (D–F) respectively in the same color schemes.

3.9.1. Bacterial Targets

Overall, the generated RMSD plot for *E. coli*-DHPS and *S. aureus*-DHFR complexed with **CB18** and **F9** were quite stable and remain converged between ~ 0.75 Å. This stability was evident with the stable conformation of the ligand inside the binding pocket during the entire simulation period (Figure 3). The 3D-conformations of **CB18** and **F9** were found deep inside the binding pocket together with the corresponding co-crystallized pteronic acid [57] and [58] in *E. coli*-DHPS and *S. aureus*-DHFR, respectively (Figure 3A,D).

The 2D interaction analysis after 20 ns revealed the contribution of fumarate moiety in establishing H-bonds (<3 Å distance), while 2-ethylhexyl and 2-ethyloctyl through hydrophobic interactions with the binding site residues of *E. coli*-DHPS and *S. aureus*-DHFR respectively. The fumarate moiety interacted through H-bonds with common residues, including Asn22, Arg63 and Arg255, whereas **F9** established additional H-bonds with Thr62 and His257 (Figure 3B). Likewise, with DHFR, Asn19 and Gln20 were commonly interacted through H-bonds, while the additional H-bond was observed in **F9** and **CB18** with Ala8 and Phe17 residues. Apart from H-bonds, a large number of conserved hydrophobic interactions were also observed including Ile20, Gly58, Glu60, Ser61, Pro64, Met148, Phe188, Gly189, Phe190, and Lys221 in *E. coli*-DHPS, whereas Ile15, Gly16, Leu21, Thr47, Ser50, Phe93, Gly94, Gly95, and Phe99 in *S. aureus*-DHFR.

3.9.2. Enzymatic Targets

The RMSD trajectory plots of corresponding enzymes with bound ligands showed a similar trend, where the complexes remained converge between 0.75 – 1.25 Å in AChE and *S. cerevisiae*- α -glucosidase. Both compounds were found to have a similar binding pose deep inside the hydrophobic groove of both enzymes when superimposed on reported co-crystallized complexes [55] (Figure 4A,D). Likewise, in the interaction of **CB18** and **F9** with other bacterial targets (Figure 3B,E), fumarate moiety actively contributed in H-bond interactions (<3 Å distance) with conserved residues, including Thr83, Ser125

and Tyr341 in AChE, where **F9** established one additional H-bond with Tyr124 (Figure 4B). With α -Glucosidase, His111, Asp214, Arg439 were revealed conserve residues in establishing H-bonds with both ligands whereas **CB18** established additional H-bonds with His348 and Arg212 (Figure 4E).

3.10. MMGBSA Binding Free Energy Calculations

To further explore the binding free energy calculations between selected proteins with **CB18** and **F9** compounds separately, MMGBSA calculations were performed. The MMGBSA total energy (ΔG_{tol}) was divided into molecular mechanics (ΔE_{MM}) and solvation energy (ΔG_{sol}) contributions. ΔE_{ele} is further divided into van der Waals (ΔE_{vdw}) and electrostatic energy contributions (ΔE_{ele}) while solvation energy is divided into polar (ΔG_{p}) and nonpolar (ΔG_{np}) contributions. A total of 1000 snapshots were extracted from the whole trajectory for binding free energy calculations. The predicted total binding affinities and contributing energies are tabulated in Table 6.

Table 6. Binding affinities and contributing energies of the isolates.

Identified Targets	Bioactive Compounds	ΔE_{vdw}	ΔE_{ele}	ΔE_{MM}	ΔG_{p}	ΔG_{np}	ΔG_{sol}	ΔG_{tol}
AChE	CB18	−40.05	−8.67	−48.72	23.89	−3.46	20.43	−28.29
	F9	−39.98	−9.56	−49.54	22.13	−4.11	18.02	−31.52
Glucosidase	CB18	−45.64	−10.21	−55.85	23.68	−7.69	15.99	−39.86
	F9	−43.54	−11.33	−54.87	26.39	−6.44	19.95	−34.92
DHPS (<i>E. coli</i>)	CB18	−24.2	−8.27	−32.47	16.41	−2.64	13.77	−18.7
	F9	−21	−5.61	−26.61	17.03	−3.21	13.82	−12.79
DHFR (<i>S. aureus</i>)	CB18	−28.44	−5.25	−33.69	20.26	−4.32	15.94	−17.75
	F9	−26.21	−4.22	−30.43	21.59	−5.89	15.7	−14.73

The MMGBSA calculations along with molecular mechanics (ΔE_{MM}) and solvation energy (ΔG_{sol}) contributions are tabulated in Table 6. The estimated MMGBSA values for the targets were slightly consistent with the experimental results. For instance, the MMGBSA binding free energy was very promising with both compounds, **CB18** and **F9** against α -GluE ($\Delta G_{\text{tol}} = -39.86$ kcal/mol; $\Delta G_{\text{tol}} = -34.92$ kcal/mol), the results were apparent with reasonable 43.82% (**CB18**) and 42.35% (**F9**) enzyme inhibition activity with respect to Acarbose (standard drug) (92.23%) at a concentration of 0.5 mM. While, with antibacterial potential targets, **CB18** and **F9** revealed lower ΔG_{tol} with *E. coli* DHPS ($\Delta G_{\text{tol}} = -18.7$ kcal/mol and $\Delta G_{\text{tol}} = -12.79$ kcal/mol) and *S. aureus* DHFR ($\Delta G_{\text{tol}} = -17.75$ kcal/mol and $\Delta G_{\text{tol}} = -14.73$ kcal/mol) which were evident from less significant antibacterial activity of both compounds (**CB18** and **F9**) against *E. coli* (i.e., 11.33% and 14.33%) and *S. aureus* (i.e., 14% and 10%) as compared to ampicillin (90% and 95%) at 1 mg/mL, respectively. Likewise, the estimated ΔG_{tol} of **CB18** and **F9** with AChE also showed higher binding energy ($\Delta G_{\text{tol}} = -28.29$ kcal/mol and $\Delta G_{\text{tol}} = -31.52$ kcal/mol).

4. Conclusions

Through bioassay direction, two maleates were isolated from *P. cretica* and their structures were elucidated. Target potentials were evaluated by reverse docking and biological potentials of the isolates were measured for best-targeted potentials. The results show that the isolates are moderately active against all tested activities. Consequently, it can be said that the isolates have poly-pharmacological potentials. Further study is required to fully explore this plant species.

Supplementary Materials: The following are available online at <http://www.mdpi.com/2076-3921/8/7/231/s1>, Table S1. Detailed absorption, distribution, metabolism, toxicity and excretion in silico assessment.

Author Contributions: Conceptualization, I.A., M.U.M. and S.A.; Formal analysis, F.S., R.M., S.M., M.T.J.K., Z.-u.-D.K., M.A. and M.S.A.; Investigation, R.M.; Methodology, F.S., M.T.J.K., Z.-u.-D.K., M.A. and S.A.; Resources, M.S.A., I.A. and M.U.M.; Supervision, S.A.; Validation, R.M.; Visualization, F.S.; Writing—original draft, F.S. and M.U.M.; Writing—review & editing, M.T.J.K., M.F. and S.A.

Funding: This research received no external funding.

Conflicts of Interest: The authors declare no conflict of interest.

References

1. Raghavendra, M.; Satish, S.; Raveesha, K. Phytochemical analysis and antibacterial activity of *Oxalis corniculata*; a known medicinal plant. *Myscience* **2006**, *1*, 72–78.
2. Şahin, F.; Karaman, I.; Güllüce, M.; Ögütçü, H.; Şengül, M.; Adıgüzel, A.; Öztürk, S.; Kotan, R. Evaluation of antimicrobial activities of *Satureja hortensis* L. *J. Ethnopharmacol.* **2003**, *87*, 61–65. [[CrossRef](#)]
3. Newman, D.J.; Cragg, G.M. Natural Products as Sources of New Drugs from 1981 to 2014. *J. Nat. Prod.* **2016**, *79*, 629–661. [[CrossRef](#)] [[PubMed](#)]
4. Zhang, L.; Rothfels, C.J.; Ebihara, A.; Schuettelpelz, E.; Le Péchon, T.; Kamau, P.; He, H.; Zhou, X.-M.; Prado, J.; Field, A.; et al. A global plastid phylogeny of the brake fern genus *Pteris* (*Pteridaceae*) and related genera in the *Pteridoideae*. *Cladistics* **2015**, *31*, 406–423. [[CrossRef](#)]
5. Pratibha, K.; Otaghvari, A.M.; Govindaparyi, H.; Bahuguna, Y.M.; Uniyal, P. Some ethno-medicinally important pteridophytes of India. *Int. J. Med. Arom. Plants* **2011**, *1*, 18–22.
6. Imperato, F. Luteolin 8-C-rhamnoside-7-O-rhamnoside from *Pteris cretica*. *Phytochemistry* **1994**, *37*, 589–590. [[CrossRef](#)]
7. Saleem, F.; Khan, M.T.J.; Saleem, H.; Azeem, M.; Ahmed, S.; Shahid, N.; Altaf, H. Phytochemical, antimicrobial and antioxidant activities of *Pteris cretica* L. (*Pteridaceae*) extracts. *Acta. Pol. Pharm.* **2016**, *73*, 1397–1403. [[PubMed](#)]
8. Diopan, V.; Babula, P.; Shestivska, V.; Adam, V.; Zemlicka, M.; Dvorska, M.; Hubalek, J.; Trnkova, L.; Havel, L.; Kizek, R. Electrochemical and spectrometric study of antioxidant activity of pomiferin, isopomiferin, osajin and catalposide. *J. Pharm. Biomed. Anal.* **2008**, *48*, 127–133. [[CrossRef](#)]
9. Wondrak, G.T.; Villeneuve, N.F.; Lamore, S.D.; Bause, A.S.; Jiang, T.; Zhang, D.D. The cinnamon-derived dietary factor cinnamic aldehyde activates the Nrf2-dependent antioxidant response in human epithelial colon cells. *Molecules* **2010**, *15*, 3338–3355. [[CrossRef](#)]
10. Adams, R.; Craig, P.; Parsons, O. Neuropsychology of dementia. *Neurol. Clin.* **1986**, *4*, 387–404. [[CrossRef](#)]
11. Orhan, I.; Şener, B.; Choudhary, M.; Khalid, A. Acetylcholinesterase and butyrylcholinesterase inhibitory activity of some Turkish medicinal plants. *J. Ethnopharmacol.* **2004**, *91*, 57–60. [[CrossRef](#)] [[PubMed](#)]
12. Hung, C.L.; Chen, C.C. Computational approaches for drug discovery. *Drug Dev. Res.* **2014**, *75*, 412–418. [[CrossRef](#)] [[PubMed](#)]
13. Katsila, T.; Spyroulias, G.A.; Patrinos, G.P.; Matsoukas, M.T. Computational approaches in target identification and drug discovery. *Comput. Struct. Biotechnol. J.* **2016**, *14*, 177–184. [[CrossRef](#)] [[PubMed](#)]
14. Macalino, S.J.; Gosu, V.; Hong, S.; Choi, S. Role of computer-aided drug design in modern drug discovery. *Arch. Pharm. Res.* **2015**, *38*, 1686–1701. [[CrossRef](#)] [[PubMed](#)]
15. Xu, X. New concepts and approaches for drug discovery based on traditional Chinese medicine. *Drug Discov. Today* **2006**, *3*, 247–253. [[CrossRef](#)]
16. Xiang, M.; Cao, Y.; Fan, W.; Chen, L.; Mo, Y. Computer-aided drug design: Lead discovery and optimization. *Comb. Chem. High Throughput Screen.* **2012**, *15*, 328–337. [[CrossRef](#)] [[PubMed](#)]
17. Ramström, O.; Lehn, J.-M. Drug discovery by dynamic combinatorial libraries. *Nat. Rev. Drug Discov.* **2002**, *1*, 26. [[CrossRef](#)]
18. Lehn, J.-M.; Eliseev, A.V. Dynamic combinatorial chemistry. *Science* **2001**, *291*, 2331–2332. [[CrossRef](#)]
19. Terrett, N.K.; Gardner, M.; Gordon, D.W.; Kobylecki, R.J.; Steele, J. Combinatorial synthesis—the design of compound libraries and their application to drug discovery. *Tetrahedron* **1995**, *51*, 8135–8173. [[CrossRef](#)]
20. Klebe, G. Virtual ligand screening: Strategies, perspectives and limitations. *Drug Discov. Today* **2006**, *11*, 580–594. [[CrossRef](#)]

21. Ma, X.H.; Jia, J.; Zhu, F.; Xue, Y.; Li, Z.R.; Chen, Y.Z. Comparative analysis of machine learning methods in ligand-based virtual screening of large compound libraries. *Comb. Chem. High Throughput Screen.* **2009**, *12*, 344–357. [[CrossRef](#)] [[PubMed](#)]
22. Waszkowycz, B. Structure-based approaches to drug design and virtual screening. *Curr. Opin. Drug Discov. Devel.* **2002**, *5*, 407–413. [[PubMed](#)]
23. Cheng, T.; Li, Q.; Zhou, Z.; Wang, Y.; Bryant, S.H. Structure-based virtual screening for drug discovery: A problem-centric review. *AAPS J.* **2012**, *14*, 133–141. [[CrossRef](#)] [[PubMed](#)]
24. Ekins, S.; Mestres, J.; Testa, B. In silico pharmacology for drug discovery: Methods for virtual ligand screening and profiling. *Br. J. Pharmacol.* **2007**, *152*, 9–20. [[CrossRef](#)] [[PubMed](#)]
25. Kumar, A.; Zhang, K.Y. Hierarchical virtual screening approaches in small molecule drug discovery. *Methods* **2015**, *71*, 26–37. [[CrossRef](#)] [[PubMed](#)]
26. Lavecchia, A.; Di Giovanni, C. Virtual screening strategies in drug discovery: A critical review. *Cur. Med. Chem.* **2013**, *20*, 2839–2860. [[CrossRef](#)]
27. Hui-fang, L.; Qing, S.; Jian, Z.; Wei, F. Evaluation of various inverse docking schemes in multiple targets identification. *J. Mol. Graph. Model.* **2010**, *29*, 326–330. [[CrossRef](#)]
28. Kharkar, P.S.; Warriar, S.; Gaud, R.S. Reverse docking: A powerful tool for drug repositioning and drug rescue. *Future Med. Chem.* **2014**, *6*, 333–342. [[CrossRef](#)]
29. Böttcher, T.; Pitscheider, M.; Sieber, S.A. Natural products and their biological targets: Proteomic and metabolomic labeling strategies. *Angew. Chem Int. Ed.* **2010**, *49*, 2680–2698. [[CrossRef](#)]
30. Cheng, K.W.; Wong, C.C.; Wang, M.; He, Q.Y.; Chen, F. Identification and characterization of molecular targets of natural products by mass spectrometry. *Nucleic Acids Res.* **2010**, *29*, 126–155. [[CrossRef](#)]
31. Huang, C.-M.; Elmets, C.A.; De-chu, C.T.; Li, F.; Yusuf, N. Proteomics reveals that proteins expressed during the early stage of *Bacillus anthracis* infection are potential targets for the development of vaccines and drugs. *Genom. Proteom. Bioinform.* **2004**, *2*, 143–151. [[CrossRef](#)]
32. Li, H.; Zheng, M.; Liu, X.; Jiang, H. Computational Approach for Drug Target Identification. *Chem. Genom.* **2012**, 279.
33. Liu, X.; Ouyang, S.; Yu, B.; Liu, Y.; Huang, K.; Gong, J.; Zheng, S.; Li, Z.; Li, H.; Jiang, H. PharmMapper server: A web server for potential drug target identification using pharmacophore mapping approach. *Nucleic Acids Res.* **2010**, *38*, W609–W614. [[CrossRef](#)] [[PubMed](#)]
34. Kinnings, S.L.; Jackson, R.M. ReverseScreen3D: A structure-based ligand matching method to identify protein targets. *J. Chem. Inf. Model.* **2011**, *51*, 624–634. [[CrossRef](#)] [[PubMed](#)]
35. Chen, Y.; Ung, C. Prediction of potential toxicity and side effect protein targets of a small molecule by a ligand–protein inverse docking approach. *J. Mol. Graph. Model.* **2001**, *20*, 199–218. [[CrossRef](#)]
36. Li, H.; Gao, Z.; Kang, L.; Zhang, H.; Yang, K.; Yu, K.; Luo, X.; Zhu, W.; Chen, K.; Shen, J.; et al. TarFisDock: A web server for identifying drug targets with docking approach. *Nucleic Acids Res.* **2006**, *34*, W219–W224. [[CrossRef](#)] [[PubMed](#)]
37. Wang, J.-C.; Chu, P.-Y.; Chen, C.-M.; Lin, J.-H. idTarget: A web server for identifying protein targets of small chemical molecules with robust scoring functions and a divide-and-conquer docking approach. *Nucleic Acids Res.* **2012**, *40*, W393–W399. [[CrossRef](#)]
38. Wang, L.; Ma, C.; Wipf, P.; Liu, H.; Su, W.; Xie, X.-Q. TargetHunter: An in silico target identification tool for predicting therapeutic potential of small organic molecules based on chemogenomic database. *AAPS J.* **2013**, *15*, 395–406. [[CrossRef](#)]
39. Zheng, R.; Chen, T.-S.; Lu, T. A comparative reverse docking strategy to identify potential antineoplastic targets of tea functional components and binding mode. *Int. J. Mol. Sci.* **2011**, *12*, 5200–5212. [[CrossRef](#)]
40. Bhattacharjee, B.; Vijayasathy, S.; Karunakar, P.; Chatterjee, J. Comparative reverse screening approach to identify potential anti-neoplastic targets of saffron functional components and binding mode. *Asian Pac. J. Cancer Prev.* **2012**, *13*, 5605–5611. [[CrossRef](#)]
41. Bhattacharjee, B.; Chatterjee, J. Identification of proapoptotic, anti-inflammatory, anti-proliferative, anti-invasive and anti-angiogenic targets of essential oils in cardamom by dual reverse virtual screening and binding pose analysis. *Asian Pac. J. Cancer Prev.* **2013**, *14*, 3735–3742. [[CrossRef](#)] [[PubMed](#)]
42. Kumar, R.P.; Manoj, M.; Kush, A.; Annadurai, R. In silico approach of azadirachtin binding with actins. *Insect Biochem. Mol. Biol.* **2007**, *37*, 635–640. [[CrossRef](#)] [[PubMed](#)]

43. Kiss, R.; Szalai, F.; Sandor, M. Molecule.com: A public web service for drug discovery. *Abstr. Pap. Am. Chem. Soc.* **2012**, *243*. [[CrossRef](#)]
44. Cheng, F.; Li, W.; Zhou, Y.; Shen, J.; Wu, Z.; Liu, G.; Lee, P.W.; Tang, Y. admetSAR: A comprehensive source and free tool for assessment of chemical ADMET properties. *J. Chem. Inf. Model.* **2012**, *52*, 3099–3105. [[CrossRef](#)] [[PubMed](#)]
45. Liu, T.; Lin, Y.; Wen, X.; Jorissen, R.N.; Gilson, M.K. BindingDB: A web-accessible database of experimentally determined protein–ligand binding affinities. *Nucleic Acids Res.* **2006**, *35*, D198–D201. [[CrossRef](#)] [[PubMed](#)]
46. Wishart, D.S.; Knox, C.; Guo, A.C.; Shrivastava, S.; Hassanali, M.; Stothard, P.; Chang, Z.; Woolsey, J. DrugBank: A comprehensive resource for in silico drug discovery and exploration. *Nucleic Acids Res.* **2006**, *34*, D668–D672. [[CrossRef](#)] [[PubMed](#)]
47. Gao, Z.; Li, H.; Zhang, H.; Liu, X.; Kang, L.; Luo, X.; Zhu, W.; Chen, K.; Wang, X.; Jiang, H. PDPTD: A web-accessible protein database for drug target identification. *BMC Bioinform.* **2008**, *9*, 104. [[CrossRef](#)] [[PubMed](#)]
48. Wang, Y.; Bolton, E.; Dracheva, S.; Karapetyan, K.; Shoemaker, B.A.; Suzek, T.O.; Wang, J.; Xiao, J.; Zhang, J.; Bryant, S.H. An overview of the PubChem BioAssay resource. *Nucleic Acids Res.* **2009**, *38*, D255–D266. [[CrossRef](#)]
49. Mangal, M.; Sagar, P.; Singh, H.; Raghava, G.P.; Agarwal, S.M. NPACT: Naturally occurring plant-based anti-cancer compound-activity-target database. *Nucleic Acids Res.* **2012**, *41*, D1124–D1129. [[CrossRef](#)] [[PubMed](#)]
50. Ye, H.; Ye, L.; Kang, H.; Zhang, D.; Tao, L.; Tang, K.; Liu, X.; Zhu, R.; Liu, Q.; Chen, Y.Z.; et al. HIT: Linking herbal active ingredients to targets. *Nucleic Acids Res.* **2010**, *39*, D1055–D1059. [[CrossRef](#)] [[PubMed](#)]
51. Sarker, S.D.; Nahar, L.; Kumarasamy, Y. Microtitre plate-based antibacterial assay incorporating resazurin as an indicator of cell growth, and its application in the in vitro antibacterial screening of phytochemicals. *Methods* **2007**, *42*, 321–324. [[CrossRef](#)] [[PubMed](#)]
52. Taha, M.; Ismail, N.H.; Khan, A.; Shah, S.A.A.; Anwar, A.; Halim, S.A.; Fatmi, M.Q.; Imran, S.; Rahim, F.; Khan, K.M. Synthesis of novel derivatives of oxindole, their urease inhibition and molecular docking studies. *Bioorg. Med. Chem. Lett.* **2015**, *25*, 3285–3289. [[CrossRef](#)] [[PubMed](#)]
53. Chapdelaine, P.; Tremblay, R.R.; Dube, J. P-Nitrophenol-alpha-D-glucopyranoside as substrate for measurement of maltase activity in human semen. *Clin. Chem.* **1978**, *24*, 208–211. [[PubMed](#)]
54. Trott, O.; Olson, A.J. AutoDock Vina: Improving the speed and accuracy of docking with a new scoring function, efficient optimization, and multithreading. *J. Comput. Chem.* **2010**, *31*, 455–461. [[CrossRef](#)] [[PubMed](#)]
55. Nachon, F.; Carletti, E.; Ronco, C.; Trovaslet, M.; Nicolet, Y.; Jean, L.; Renard, P.-Y. Crystal structures of human cholinesterases in complex with huprine W and tacrine: Elements of specificity for anti-Alzheimer's drugs targeting acetyl- and butyryl-cholinesterase. *Biochem. J.* **2013**, *453*, 393–399. [[CrossRef](#)] [[PubMed](#)]
56. Schwede, T.; Kopp, J.; Guex, N.; Peitsch, M.C. SWISS-MODEL: An automated protein homology-modeling server. *Nucleic Acids Res.* **2003**, *31*, 3381–3385. [[CrossRef](#)] [[PubMed](#)]
57. Dennis, M.L.; Lee, M.D.; Harjani, J.R.; Ahmed, M.; DeBono, A.J.; Pitcher, N.P.; Wang, Z.C.; Chhabra, S.; Barlow, N.; Rahmani, R.; et al. 8-Mercaptoguanine Derivatives as Inhibitors of Dihydropteroate Synthase. *Chem. Eur. J.* **2018**, *24*, 1922–1930. [[CrossRef](#)] [[PubMed](#)]
58. Lam, T.; Hilgers, M.T.; Cunningham, M.L.; Kwan, B.P.; Nelson, K.J.; Brown-Driver, V.; Ong, V.; Trzoss, M.; Hough, G.; Shaw, K.J.; et al. Structure-based design of new dihydrofolate reductase antibacterial agents: 7-(benzimidazol-1-yl)-2,4-diaminoquinazolines. *J. Med. Chem.* **2014**, *57*, 651–668. [[CrossRef](#)] [[PubMed](#)]
59. Ahmed, B.; Ali Ashfaq, U.; Usman Mirza, M. Medicinal plant phytochemicals and their inhibitory activities against pancreatic lipase: Molecular docking combined with molecular dynamics simulation approach. *Nat. Pro. Res.* **2018**, *32*, 1123–1129. [[CrossRef](#)]
60. Ferdous, S.; Mirza, M.U.; Saeed, U. Docking studies reveal phytochemicals as the long searched anticancer drugs for breast cancer. *Int. J. Comp. Appl.* **2013**, *67*, 1–5. [[CrossRef](#)]
61. Yousuf, Z.; Iman, K.; Iftikhar, N.; Mirza, M.U. Structure-based virtual screening and molecular docking for the identification of potential multi-targeted inhibitors against breast cancer. *Breast Cancer (Dove Med. Press)* **2017**, *9*, 447–459. [[CrossRef](#)] [[PubMed](#)]

62. Pettersen, E.F.; Goddard, T.D.; Huang, C.C.; Couch, G.S.; Greenblatt, D.M.; Meng, E.C.; Ferrin, T.E. UCSF Chimera—A visualization system for exploratory research and analysis. *J. Comput. Chem.* **2004**, *25*, 1605–1612. [[CrossRef](#)] [[PubMed](#)]
63. Case, D.A.; Cheatham, T.E., III; Darden, T.; Gohlke, H.; Luo, R.; Merz, K.M., Jr.; Onufriev, A.; Simmerling, C.; Wang, B.; Woods, R.J. The Amber biomolecular simulation programs. *J. Comput. Chem.* **2005**, *26*, 1668–1688. [[CrossRef](#)] [[PubMed](#)]
64. Iman, K.; Mirza, M.U.; Mazhar, N.; Vanmeert, M.; Irshad, I.; Kamal, M.A. In silico Structure-based Identification of Novel Acetylcholinesterase Inhibitors Against Alzheimer’s Disease. *CNS Neurol. Disord. Drug Targets* **2018**, *17*, 54–68. [[CrossRef](#)]
65. Roe, D.R.; Cheatham, T.E., III. PTRAJ and CPPTRAJ: Software for processing and analysis of molecular dynamics trajectory data. *J. Chem. Theory Comput.* **2013**, *9*, 3084–3095. [[CrossRef](#)]
66. Gohlke, H.; Kiel, C.; Case, D.A. Insights into protein–protein binding by binding free energy calculation and free energy decomposition for the Ras–Raf and Ras–RalGDS complexes. *J. Mol. Biol.* **2003**, *330*, 891–913. [[CrossRef](#)]
67. Hayes, J.M.; Archontis, G. MM-GB (PB) SA calculations of protein–ligand binding free energies. In *Molecular Dynamics-Studies of Synthetic and Biological Macromolecules*; Wang, L., Ed.; InTech: Rijeka, Croatia, 2012.
68. Herbst, R.S. Review of epidermal growth factor receptor biology. *Int. J. Radiat. Oncol. Biol. Phys.* **2004**, *59*, S21–S26. [[CrossRef](#)] [[PubMed](#)]
69. Ciardiello, F. Epidermal growth factor receptor tyrosine kinase inhibitors as anticancer agents. *Drugs* **2000**, *60*, 25–32. [[CrossRef](#)]
70. Lai, C.-J.; Bao, R.; Tao, X.U.; Wang, J.; Atoyan, R.; Qu, H.; Wang, D.G.; Yin, L.; Samson, M.; Forrester, J.; et al. CUDC-101, a multitargeted inhibitor of histone deacetylase, epidermal growth factor receptor, and human epidermal growth factor receptor 2, exerts potent anticancer activity. *Can. Res.* **2010**, *70*, 3647–3656. [[CrossRef](#)]
71. Tamm, I.; Wang, Y.; Sausville, E.; Scudiero, D.A.; Vigna, N.; Oltersdorf, T.; Reed, J.C. IAP-family protein survivin inhibits caspase activity and apoptosis induced by Fas (CD95), Bax, caspases, and anticancer drugs. *Can. Res.* **1998**, *58*, 5315–5320.
72. Stewart, Z.A.; Westfall, M.D.; Pietenpol, J.A. Cell-cycle dysregulation and anticancer therapy. *Trends Pharmacol. Sci.* **2003**, *24*, 139–145. [[CrossRef](#)]
73. Sanchez-Martinez, C.; Gelbert, L.M.; Lallena, M.J.; de Dios, A. Cyclin dependent kinase (CDK) inhibitors as anticancer drugs. *Bioorg. Med. Chem. Lett.* **2015**, *25*, 3420–3435. [[CrossRef](#)] [[PubMed](#)]
74. Rakoff-Nahoum, S. Cancer Issue: Why cancer and inflammation? *Yale J. Biol. Med.* **2006**, *79*, 123. [[PubMed](#)]
75. Gupta, S.C.; Kim, J.H.; Prasad, S.; Aggarwal, B.B. Regulation of survival, proliferation, invasion, angiogenesis, and metastasis of tumor cells through modulation of inflammatory pathways by nutraceuticals. *Cancer Metastasis Rev.* **2010**, *29*, 405–434. [[CrossRef](#)] [[PubMed](#)]
76. Kaminska, B. MAPK signalling pathways as molecular targets for anti-inflammatory therapy—from molecular mechanisms to therapeutic benefits. *Biochim. Biophys. Acta. Prot. Proteom.* **2005**, *1754*, 253–262. [[CrossRef](#)] [[PubMed](#)]
77. Yadav, D.K.; Meena, A.; Srivastava, A.; Chanda, D.; Khan, F.; Chattopadhyay, S. Development of QSAR model for immunomodulatory activity of natural coumarinolignoids. *Drug Des. Devel. Ther.* **2010**, *4*, 173.
78. Hardy, J.; Allsop, D. Amyloid deposition as the central event in the aetiology of Alzheimer’s disease. *Trends Pharmacol. Sci.* **1991**, *12*, 383–388. [[CrossRef](#)]
79. Ghosh, A.K.; Brindisi, M.; Tang, J. Developing β -secretase inhibitors for treatment of Alzheimer’s disease. *J. Neurochem.* **2012**, *120*, 71–83. [[CrossRef](#)]
80. Hoozemans, J.; Rozemuller, J.; Van Haastert, E.; Veerhuis, R.; Eikelenboom, P. Cyclooxygenase-1 and-2 in the different stages of Alzheimer’s disease pathology. *Curr. Pharm. Des.* **2008**, *14*, 1419–1427. [[CrossRef](#)]
81. Ruffi, M.S.; Aisen, P.S. Advances in Alzheimer’s disease drug development. *BMC Med.* **2015**, *13*, 62. [[CrossRef](#)]
82. Ploia, C.; Antoniou, X.; Scip, A.; Grande, V.; Cardinetti, D.; Colombo, A.; Canu, N.; Benussi, L.; Ghidoni, R.; Forloni, G.; et al. JNK plays a key role in tau hyperphosphorylation in Alzheimer’s disease models. *J. Alzheimers Dis.* **2011**, *26*, 315–329. [[CrossRef](#)] [[PubMed](#)]
83. Wang, J.Z.; Grundke-Iqbal, I.; Iqbal, K. Kinases and phosphatases and tau sites involved in Alzheimer neurofibrillary degeneration. *Eur. J. Neurosci.* **2007**, *25*, 59–68. [[CrossRef](#)] [[PubMed](#)]

84. Inestrosa, N.C.; Alvarez, A.; Perez, C.A.; Moreno, R.D.; Vicente, M.; Linker, C.; Casanueva, O.I.; Soto, C.; Garrido, J. Acetylcholinesterase accelerates assembly of amyloid- β -peptides into Alzheimer's fibrils: Possible role of the peripheral site of the enzyme. *Neuron* **1996**, *16*, 881–891. [[CrossRef](#)]
85. Tsurkan, L.G.; Hatfield, M.J.; Edwards, C.C.; Hyatt, J.L.; Potter, P.M. Inhibition of human carboxylesterases hCE1 and hiCE by cholinesterase inhibitors. *Chem. Biol. Interact.* **2013**, *203*, 226–230. [[CrossRef](#)] [[PubMed](#)]
86. Robert Norman Jones, G. The Alzheimer pandemic: Is paracetamol to blame? *Inflamm. Allergy Drug Targets* **2014**, *13*, 2–14. [[CrossRef](#)]
87. Tobinick, E.; Gross, H.; Weinberger, A.; Cohen, H. TNF-alpha modulation for treatment of Alzheimer's disease: A 6-month pilot study. *Med. Gen. Med.* **2006**, *8*, 25.
88. Heckman, P.; Wouters, C.; Prickaerts, J. Phosphodiesterase inhibitors as a target for cognition enhancement in aging and Alzheimer's disease: A translational overview. *Curr. Pharm. Des.* **2015**, *21*, 317–331. [[CrossRef](#)]



© 2019 by the authors. Licensee MDPI, Basel, Switzerland. This article is an open access article distributed under the terms and conditions of the Creative Commons Attribution (CC BY) license (<http://creativecommons.org/licenses/by/4.0/>).